An Experimental Investigation of Digging Via Localized Fluidization, Tested With RoboClam: A Robot Inspired by Atlantic Razor Clams

Citation: Isava, Monica, and Amos G. Winter V. "An Experimental Investigation of Digging Via Localized Fluidization, Tested With RoboClam: A Robot Inspired by Atlantic Razor Clams." Journal of Mechanical Design 138, 12 (September 2016): 125001 © 2016 ASME

As Published: http://dx.doi.org/10.1115/1.4034218

Publisher: ASME International

Persistent URL: http://hdl.handle.net/1721.1/120070

Version: Final published version: final published article, as it appeared in a journal, conference proceedings, or other formally published context

An Experimental Investigation of Digging Via Localized Fluidization, Tested With RoboClam: A Robot Inspired by Atlantic Razor Clams

Monica Isava
Global Engineering and Research Laboratory,
Department of Mechanical Engineering,
Massachusetts Institute of Technology,
Cambridge, MA 02139
e-mail: misava@mit.edu

Amos G. Winter V[1]
Assistant Professor
Global Engineering and Research Laboratory,
Department of Mechanical Engineering,
Massachusetts Institute of Technology,
Cambridge, MA 02139
e-mail: awinter@mit.edu

The Atlantic razor clam, Ensis directus*, burrows underwater by expanding and contracting its valves to fluidize the surrounding soil. Its digging method uses an order of magnitude less energy than would be needed to push the clam directly into soil, which could be useful in applications such as anchoring and sensor placement. This paper presents the theoretical basis for the timescales necessary to achieve such efficient digging and gives design parameters for a device to move at these timescales. It then uses RoboClam, a robot designed to imitate the razor clam's movements, to test the design rules. It was found that the minimum contraction time is the most critical timescale for efficient digging and that efficient expansion times vary more widely. The results of this paper can be used as design rules for other robot architectures for efficient digging, optimized for the size scale and soil type of the application.* [DOI: 10.1115/1.4034218]

1 Introduction and Background

Burrowing into subsea soil is challenging in many engineering applications, including anchoring, sensor placement, cable installation, and mine detonation. Traditional methods of forcibly pushing a body into soil encounter frictional forces that result in insertion energy scaling with depth squared. However, several organisms in the animal world have found alternative ways to dig using less energy. One such animal, the Atlantic razor clam (*Ensis directus*), burrows by using a series of simple valve contractions to fluidize the soil around it [1]. The aim of this research is to define design rules and parameters for a bioinspired machine that imitates *E. directus* and use localized soil fluidization to dig into soil with an order of magnitude less energy than would be required to push a blunt body to a desired depth.

In a Newtonian fluid, viscosity and density remain relatively constant with depth. Therefore, the force required to push a blunt body into the fluid also remains constant. This constant force corresponds to an insertion energy, $E = \int F(z)dz$, that scales linearly with depth. Contrastingly, in a particulate solid (like soil), there are contact stresses between particles that cause frictional forces that scale with the surrounding pressure, resulting in shear strength (and insertion force) that increases linearly with depth [2,3]. Since the insertion force increases linearly with depth, when it is integrated over depth, it results in an insertion energy that increases with depth squared. These high-energy demands can pose limits for many subsea applications, particularly those that operate on limited energy sources, such as underwater robotics.

Many animals have developed methods of burrowing into underwater soil efficiently [4–6]. Clam worms (*N. virens*) create tunnel systems in elastic muds using crack propagation [7]. The Japanese eel (*A. japonica*) uses oscillatory motions to create underwater horizontal burrows [8]. The snake blenny (*L. lampretaeformis*) uses its head to probe sand and follows with a wave-like pattern to create similar horizontal burrows [9]. Nematodes (*C. elegans*) also use undulatory motion to move efficiently in saturated media [10,11].

The Atlantic razor clam (*E. directus*) burrows into soil using a valve contraction and expansion pattern depicted in Fig. 1 [12,13]. These movements were studied in depth by E. R. Trueman, who measured the forces, stiffnesses, angles, and pressures involved in *E. directus*'s digging cycle [14]. Adapting these results, an upper bound estimate of the energy needed to dig can be calculated to be 0.21 J/cm; at this level, the energy for a razor clam to dig to its burrow depth is ten times less than the energy required to push the animal's shell the same distance in static soil [15]. Additionally, *E. directus* can only produce 10 N of force to pull its valves into soil, which, if it were used to push a blunt body, would only result in 1–2 cm of digging [1,14]. However, razor clams can dig up to 70 cm deep [16]. This energy-to-distance ratio equates to *E. directus* being able to travel over half a kilometer using only the energy in an AA battery [17]. *E. directus* achieves this very efficient digging by contracting its valves to fluidize the soil around its body, which results in drastic drag and energy reductions for the razor clam [18]. Because of the simplicity of its movements, as well as the low-energy requirements for digging, the Atlantic razor clam is a good candidate for biomimicry [19].

This paper explores the fluid, solid, and soil mechanics relevant to the process of soil fluidization, as well as the design decisions that went into creating an *E. directus*-inspired robot, RoboClam. It then describes the testing that was conducted on RoboClam to validate the soil fluidization model and discusses insights given by the results. It concludes with comments on how the theory presented in this paper could be used to design RoboClam-inspired machines for different size scales and soil types.

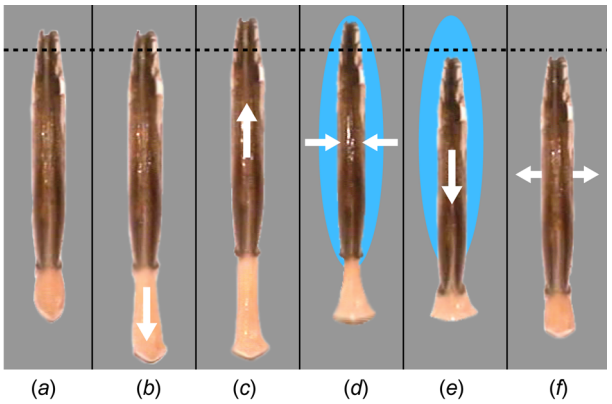

Fig. 1 *E. directus* digging pattern. Dashed horizontal line denotes a reference depth, white arrows denote clam motions, blue shaded area represents fluidized soil around the animal. (*a*) Reference position before beginning the digging cycle. (*b*) *E. directus* extends its foot down prior to moving its valves. (*c*) *E. directus* moves its valves slightly up before contraction. (*d*) *E. directus* contracts its valves, which fluidizes the soil around it and pushes blood into its foot. (*e*) *E. directus*'s foot pulls its valves down through the fluidized soil. (*f*) *E. directus* reopens its valves to begin another digging cycle, now at a lower depth than in part *a*.

[1]Corresponding author.

Contributed by the Mechanisms and Robotics Committee of ASME for publication in the Journal of Mechanical Design. Manuscript received October 2, 2015; final manuscript received July 8, 2016; published online September 14, 2016. Assoc. Editor: David Myszka.

2 Mechanics of Localized Soil Fluidization

When *E. directus* contracts its valves, it reduces stress in the soil to a point of failure while drawing water toward its body. The water and soil mix to form a fluidized substrate, through which the animal can move efficiently. The optimal situation (and the situation seen in *E. directus*' natural digging pattern) occurs when the valves contract at a speed that allows fluidization to occur at the same time as contraction. In this case, when contraction is complete, the surrounding substrate is fluidized and the razor clam is able to pull itself to a deeper position before expanding its valves again.

To quantify the minimum contraction time needed to achieve fluidization, one can examine the drag that keeps the soil particles from fluidizing when contraction occurs. The relevant Reynolds number for the fluid flowing into the void after contraction is $\mathrm{Re} = (\rho_f v_v d_p/\mu_f)$, where ρ_f and μ_f are the density and viscosity of the fluid, respectively, v_v is the velocity of valve contraction, and d_p is the diameter of a soil particle. This Reynolds number varies between 0.02 and 56 depending on particle size, animal size, and valve contraction velocity [15]. However, this entire Reynolds number range falls in the domain of Stokes drag [20]. Using Stokes drag and conservation of momentum, the characteristic time required for a soil particle to reach the velocity of the advecting fluid (that is, the minimum contraction time required for fluidization to occur) can be estimated as

$$m_p \frac{dv_p}{dt} = 6\pi\mu_f d_p(v_v - v_p) \quad \rightarrow \quad t_{\min} = \frac{d_p^2 \varrho_p}{36\mu_f} \tag{1}$$

where m_p is the mass of the soil particle, v_p is the velocity of the particle, μ_f is the fluid viscosity, d_p is the particle diameter, v_v is the contraction velocity of the clam's valves, ρ_p is the density of the particle, and $t_{\min}$ is the time constant of the differential equation governing velocity change in Stokes flow. As the soil particles get larger or denser, $t_{\min}$ increases, as it becomes more difficult for the particles to accelerate to the speed of the surrounding fluid. Conversely, as the fluid gets more viscous, $t_{\min}$ decreases since the fluid can exert a higher drag force on the particles and bring them up to speed faster. For 1 mm soda lime glass beads (which are similar in size and density to *E. directus*' natural environment and which were used in the experiments presented in this paper), this minimum contraction time is 0.075 s [15,21].

If the valves were to contract more quickly than $t_{\min}$ and then instantaneously expand again, the fluid would not have a chance to advect the soil particles and the particles would instead remain stationary. In this case, no fluidization would occur and the animal would remain at its original depth. If the valves were to contract more quickly than $t_{\min}$ and immediately begin to expand again, the substrate would fluidize during the animal's expansion motion rather than its contraction motion. In this situation, *E. directus* would be able to dig, but since fluidization occurs during expansion, the animal would not have a chance to dig when both its valves are completely contracted and the surrounding substrate is fluidized. Thus, digging would be less efficient than at $t_{\min}$.

3 Materials and Methods

3.1 Design of RoboClam. In order to test whether an *E. directus*-inspired machine would exhibit energy efficiency similar to that of the razor clam, as well as to test the minimum contraction time for fluidization calculated in Eq. 1, RoboClam was designed and built. The general architecture, as well as the digging pattern of RoboClam, is shown in Fig. 2. The machine consists of two pistons: one set concentrically around the other, which connect to an *E. directus*-shaped end effector. One piston connects directly to the top of the end effector and moves it up and down, and the other connects to a wedge inside the end effector, which translates vertical motion in the piston to horizontal (contraction/expansion) motion in the end effector. Pneumatics

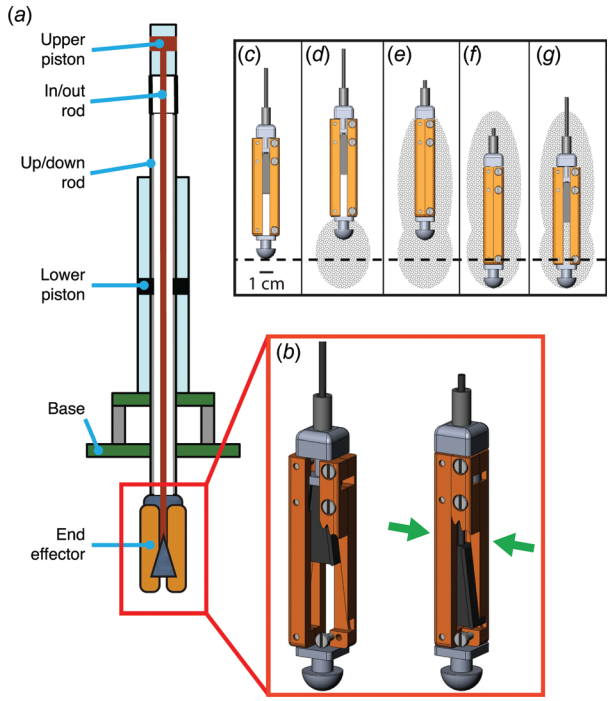

Fig. 2 RoboClam architecture and digging motions. (*a*) RoboClam architecture. The upper piston moves the end effector in and out; the lower piston moves it up and down. (*b*) Inset of the end effector. The wedge mechanism connected to the upper piston translates vertical (piston) motion to horizontal (in/out) motion. (*c–g*) RoboClam movements, which map to the *E. directus* motions shown in parts *b–f* of Fig. 1. Dotted line represents a reference depth; gray areas indicate anticipated fluidized areas.

were chosen to control the pistons so that RoboClam could be safely tested both in real ocean substrates and in controlled lab environments. Through this pneumatic control system, the robot is able to mimic *E. directus*'s digging pattern, as depicted in Figs. 2(*c*)–2(*g*).

The end effector was designed to be half the size of *E. directus* (99.7 mm long and 15.2 mm wide), but open as far (6.4 mm), to be able to test the effect of in/out displacement on burrowing. The wedge is exactly constrained and has contact lengths/widths larger than two (as shown in Fig. 3(*a*)) to prohibit jamming [22]. Additionally, the wedge intersects the center of pressure on the shell regardless of its position. This prevents the shell from exerting moments on the wedge that could increase frictional losses. During testing, the end effector was completely enclosed by a neoprene

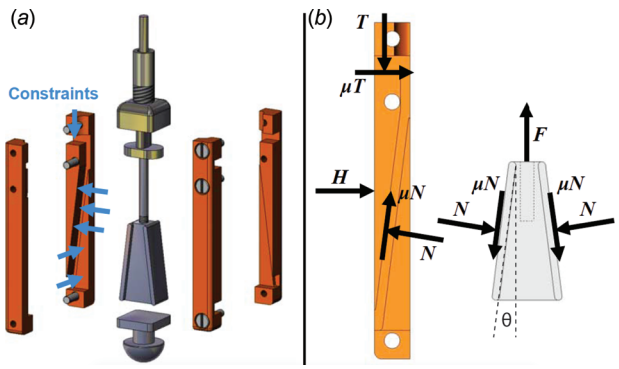

Fig. 3 RoboClam end effector design. (*a*) Exploded view of end effector, with exact constraints of shells labeled. (*b*) Free body diagram of a shell and the wedge.

boot to prevent soil particles from disturbing the end effector–wedge interface.

The transmission ratio (TR) for the mechanism can be derived from the free body diagram in Fig. 3(*b*)

$$\mathrm{TR} = \frac{H}{F} = \frac{1}{2}\left[\frac{\cos\theta - \mu\sin\theta}{\sin\theta + \mu\cos\theta} - \mu\right] \tag{2}$$

Here, F is the vertical force, H is the resultant horizontal force, θ is the angle of the wedge, and μ is the coefficient of friction between the wedge and the valves.

The theoretical efficiency of the mechanism can be found by calculating the work done over a stroke

$$\eta = \frac{E_{\mathrm{out}}}{E_{\mathrm{in}}} = 2\frac{H\delta_x}{F\delta_y} = 2\mathrm{TR}\sin\theta \tag{3}$$

The end effector was made from alloy 932 (SAE 660) bearing bronze and 440 C stainless steel, because both materials are salt-water compatible and have a low coefficient of sliding friction when lubricated [23]. The dynamic coefficient of friction within the mechanism was measured to be 0.173 with 0.013 standard deviation under horizontal loads ranging from 13.34 N to 83.74 N [24]. Silicon oil was used as a lubricant because the neoprene boot does not absorb it.

The angle of the wedge (θ) was chosen as 7.13 deg in order to maximize the contact lengths and widths between the wedge and the end effector, while allowing the end effector to maintain its predetermined size. This geometry yields a relatively high TR of 1.55, with a maximum of 1.83 and minimum of 1.33 corresponding to 6σ friction measurements. The corresponding efficiency is 39% with a minimum of 33% and a maximum of 46%. This efficiency was deemed acceptable, as the resulting configuration of the end effector provided small packaging size, jam-free operation, and the ability to calculate lost energy. If, in future, design iterations efficiency is critical, a maximum of 60% efficiency can be achieved using a similar wedge design with the same materials and a wedge angle of 29 deg [24].

3.2 Energy Expenditure Calibration. RoboClam's design was optimized to facilitate tracking of the energy spent in soil deformation while digging. Soil deformation energy can be calculated as the total input energy minus all of the other losses in the system. For RoboClam's up/down motion, the energy lost to soil deformation during one stroke is

$$\begin{aligned} E_{\mathrm{soil}} &= E_{\mathrm{in}} - E_{\mathrm{friction}} - E_{\mathrm{potential}} \\ &= \int_{\delta_1}^{\delta_2} \Delta p_u A_u dy - |F_{u,\mathrm{friction}}(\delta_2 - \delta_1)| \\ &\quad - m_u g(\delta_2 - \delta_1) \end{aligned} \tag{4}$$

where the subscript u denotes the up/down piston, δ_1 and δ_2 are the starting and ending displacements of the stroke, Δp_u is the pressure difference over the piston, A_u is the area of the piston, $F_{u,\mathrm{friction}}$ is the measured frictional force in the piston, and m_u is the total mass moving up and down [24].

For RoboClam's in/out motion, the energy lost to soil deformation during one stroke is

$$\begin{aligned} E_{\mathrm{soil}} &= \eta(E_{\mathrm{in}} - E_{\mathrm{friction}} - E_{\mathrm{potential}}) - E_{\mathrm{boot}} \\ &= \eta\left[\int_{\delta_1}^{\delta_2} \Delta p_i A_i dy - |F_{i,\mathrm{friction}}(\delta_2 - \delta_1)|\right. \\ &\quad \left. - m_i g(\delta_2 - \delta_1)\right] \end{aligned} \tag{5}$$

where the subscript i denotes the in/out piston, η is the efficiency defined in Eq. (3), δ_1 and δ_2 are the starting and ending displacements of the stroke, Δp_i is the pressure difference over the piston, A_i is the area of the piston, $F_{i,\mathrm{friction}}$ is the measured frictional force in the piston, and m_i is the total mass moving up and down. It was very difficult to measure E_{boot}, but since this energy results from the elastic deflection of the boot, it was taken to be zero over a full cycle. This is a conservative assumption, as any energy that may have been lost due to the viscoelasticity of the neoprene will appear as additional energy dissipated in the soil [24].

3.3 RoboClam Testing. Prior to this study, RoboClam had been tested briefly in *E. directus*'s natural environment, and more extensively in a 33 gallon drum filled with 1 mm soda lime glass beads (which imitate the course sand environment of the animal) [12]. In the previous drum tests, the end effector would often run out of vertical space to dig, so the 33 gallon drum was replaced with a 96 gallon drum. The smaller drum had a vibrator connected to it that resettled the beads between tests; unfortunately, this resulted in the beads at the top becoming less packed over time than the untouched beads at the bottom. In order to make the resetting process more repeatable, the vibration method was replaced by a two-step process: first, water was pumped through the bottom of the drum for 35 s to fluidize the substrate; then, the drum was vibrated for 25 s to settle the particles.

RoboClam was run through 847 tests to validate the minimum localized fluidization time calculated in Eq. 1. In these tests, the robot dug under its own weight (it only contracted and expanded) to minimize variables in the digging pattern. Contraction and expansion times were varied automatically to populate a grid of experimental in and out times. Contraction time was defined as the time from the point where the valves began to close to the time when the valves were fully closed. Expansion time was defined as the time from the end of contraction to the end of expansion. Thus, in order to vary expansion times, a pause was defined between contraction and expansion and was varied to the desired length. Contraction time was varied by adjusting the pressure in the contracting pneumatic piston using a needle valve (controlled by a stepper motor) in the path of the tube. Contraction time was varied from approximately 0.05–1.5 s, and expansion time was varied from approximately 0.05–4 s.

Each test was analyzed for digging efficiency by calculating the best-fit exponent in the power law relationship, the energy imparted to the soil and digging depth, $\alpha = (lnE/\ln\delta)$. As mentioned in Sec. 1, tests that exhibit the efficiency of blunt-body digging are expected to have insertion force increase with depth squared (and therefore have an exponent of $\alpha = 2$), whereas tests where fluidization occurs should have insertion force increase linearly with depth (and therefore have an exponent of $\alpha = 1$).

4 Results and Discussion

4.1 Results. Figure 4 shows the initial results from 847 digging tests with RoboClam (A), with a subset of the timescales zoomed in (B). The x-axis gives measured contraction time and the y-axis gives measured expansion time. Dots are grayscale coded to show the power law exponent α of each test, with dark dots corresponding to low exponents (tests exhibiting fluidization characteristics) and white dots corresponding to high exponents (tests exhibiting blunt body-like characteristics). One can see that though the power law exponent tends to increase as the contraction time increases (and gets further away from $t_{\mathrm{min}} = 0.075$ s), it never gets close to $\alpha = 2$, an inefficient/blunt body exponent that would relate to digging in static soil. These results give the impression that fluidization will occur regardless of contraction and expansion times and that the RoboClam method of digging is more efficient than blunt body digging for any timescale. However, *one* can instinctively hypothesize that there must be some point at which RoboClam is no more

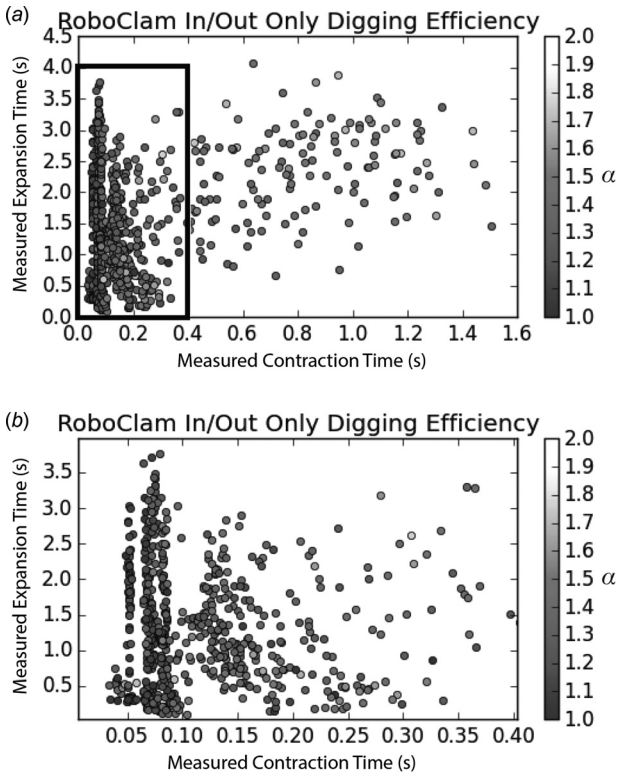

Fig. 4 Initial results from 847 digging tests on RoboClam. (*a*) Efficiency results of all 847 tests. (*b*) Subset of (A), showing greater detail on the Measured Inward Time axis. For each test, the end effector contracted and expanded at desired timescales, and the robot dug under its own weight. Tests were analyzed for the power law exponent, α, with an exponent of 1.0 corresponding to fluidized digging and 2.0 corresponding to static soil digging.

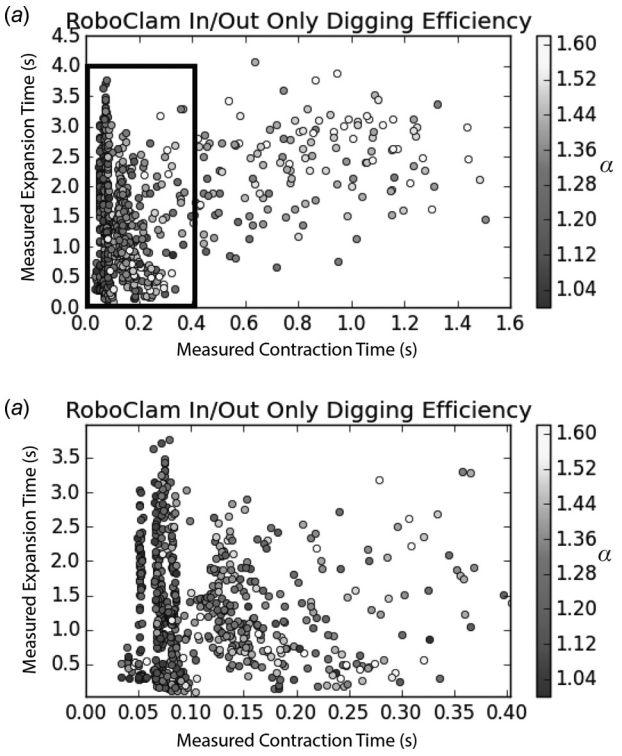

Fig. 5 Normalized results from 847 digging tests on RoboClam. (*a*) Results of all 847 tests, with a box around the zoomed in area. (*b*) Zoomed in version of (A), showing more detail on the Measured Inward Time axis. Tests were analyzed for the power law exponent, α, as in Fig. 4, but results were normalized such that an exponent of 1.0 corresponded to fluidized digging and 1.62 corresponded to blunt body digging.

effective at digging than a blunt body; if the end effector were to contract slowly enough, the substrate would collapse as contraction occurred, and there would be no void in which fluidization could occur. Thus, there is likely another phenomenon at work.

Since these results were obtained in a drum full of glass beads that were reset between tests, rather than in an untouched ocean environment, it is possible that the bead resetting methods did not completely resettle the beads between trials. That is, the fluidization and vibration used to reset the beads might have left them less packed than they would have been in an undisturbed environment. Such a situation would make it easier to dig into the beads than expected and would skew results toward fluidization, as seems to have occurred in Fig. 4.

To correct for this bias, the power law definition of a blunt body test was redefined. Rather than relying on the theory from Sec. 1, which posited that pushing a blunt body into soil would result in a power law exponent of $\alpha = 2$, the power law exponent was measured specific to the experimental setup. Fifteen tests were run in which the beads were reset using the fluidization and vibration techniques used in the other tests, then the end effector was directly pushed into the beads without moving in and out. The insertion force required from 0.025 m to 0.175 m deep was measured in 0.025 m increments. The average measured power law exponent was 1.62. Thus, the tests in Fig. 4 were normalized to a blunt body exponent of 1.62 (Fig. 5).

The results in Fig. 5 show that digging efficiency tends to be high for fast contraction times and drop off as time is increased. However, with the normalization, many tests have the same power law relationship as the blunt body pushed in static soil (shown as white dots). Therefore, Fig. 5 shows a transition across the grid between efficient and inefficient tests.

4.2 Discussion. In Fig. 5, most tests around the calculated minimum contraction time t_{min} of 0.075 s are dark, and thus exhibit fluidization, though there are some tests even below this minimum that also have low α. These results suggest that t_{min} is not a hard cutoff for localized fluidization, but rather a guideline for how quickly a razor clam-inspired machine should aim to contract to dig efficiently. In other words, if a machine is able to contract this quickly, it can be expected to achieve localized fluidization. The lack of a hard cutoff for minimum contraction time makes sense because t_{min} is calculated from a time constant, not an exact solution. The dropoff in efficiency after $t_{min} = 0.075$ s also validates the theory, derived in Sec. 2, that fluidization optimally occurs for a contraction time of approximately 0.075 s. Longer contraction times might still exhibit some fluidization, but times closer to t_{min} are preferred.

Figure 5 also shows that vertical lines of dots with contraction times below 0.10 s tend to exhibit approximately the same amount of fluidization. For example, for a contraction time of $t_{min} = 0.075$ s, the power law exponent remains at about 1.1 throughout the expansion time range of 0.05–3.8 s. In other words, there is a much larger range of acceptable expansion times than of acceptable contraction times. This phenomenon can be explained by analyzing settling time after contraction. The relevance of settling time can be understood intuitively: if the robot waited too long between contraction and expansion, the soil would settle completely, and rather than expanding back into a fluidized unpacked mixture, RoboClam would have to expand into a packed bed of soil. This expansion would cost much more energy than expansion into a fluidized body and would result in inefficient tests.

Settling time can be calculated by first using the settling velocity of a suspension of particles in fluid derived by Richardson and Zaki [25]

$$v_s = v_t \phi^n \tag{6}$$

Here, v_t is the terminal velocity of a single particle in an infinite fluid, ϕ is the void fraction of the substrate (the fraction by volume that consists of fluid or air rather than particles), and n is derived from the Archimedes number [1,26]. As the particles settle, the void fraction will decrease, and thus the settling velocity will decrease. However, to achieve a conservative estimate for settling time, the settling velocity will be kept constant in our analysis using the initial void fraction of the substrate.

The minimum void fraction required to achieve fluidization, ϕ_{fluid}, is approximately 0.41 for round particles [27]. The void fraction of settled particles for the 1 mm soda lime glass beads used in this study is $\phi_{\text{settle}} = 0.38$. If the height of the fluidized region of the substrate is defined as h_{fluid}, the settled height is

$$h_{\text{settle}} = \frac{1 - \phi_{\text{fluid}}}{1 - \phi_{\text{settle}}} h_{\text{fluid}} \tag{7}$$

Combining Eqs. (6) and (7) gives an expression for the settling time

$$t_{\text{settle}} = \frac{h_{\text{fluid}} - h_{\text{settle}}}{v_s} \tag{8}$$

Using 1 mm soda lime glass beads and defining h_{fluid} as the height of the end effector (82.1 mm) in Eq. 8 yields $t_{\text{settle}} = 2.2$ s. This is a conservative estimate because v_s was defined based only on the fluidized void fraction, so the actual settling time will be longer. Similar to the minimum contraction time t_{min}, t_{settle} is a guideline for design rather than a hard stop. The important point to note is that t_{settle} is two orders of magnitude greater than t_{min}, which suggests that when designing a RoboClam-like machine, there is much more leeway in expansion times that will achieve fluidization than in contraction times.

When designing RoboClam-inspired burrowing devices for real-world applications, if possible it would be valuable to collect soil samples in the locations where the technology would be deployed. Substrate particle size determines the critical timescales of burrowing, and some substrates may be impossible to penetrate (such as large rocks). Although the analysis and results presented in this paper pertain to granular substrates, our RoboClam robot has successfully burrowed in cohesive, silty soil with $\alpha \approx 1$ [15]. Furthermore, burrowing bivalves (including razor clams) live in a wide range of substrates, ranging from clay to coarse sand [19]. To accommodate different substrates that have not been sampled, RoboClam-inspired machines could be designed to have variable contraction times and the ability to "sense" their environment by testing different kinematic behaviors to find the one that leads to efficient digging.

5 Conclusion

This paper presents a framework for designing a robot that digs efficiently by achieving localized fluidization. RoboClam is a device that imitates *E. directus*'s digging pattern and shows that it is possible to dig efficiently like the animal. This robot gives an example of an architecture that can measure the energy used to deform soil, and thus calculate the energy efficiency of different digging patterns. It also validates the timescale guidelines for efficient digging generated by theory of fluidization and of soil settling. Using the guidelines given in this paper, a RoboClam-like device can be designed for different size scales and soil types depending on the usage scenario. Additionally, the digging timescale theory in this paper allows a designer to create other architectures that exploit localized fluidization mechanics to achieve efficient burrowing for a variety of engineering applications.

Acknowledgment

The authors would like to thank Bluefin Robotics Corporation and the MIT department of Mechanical Engineering for sponsoring this project.

Nomenclature

A_i = area of in/out piston
A_u = area of up/down piston
d_p = diameter of soil particle
E = energy
E_{boot} = energy lost to deflection of the neoprene boot
E_{friction} = energy lost to friction
E_{in} = energy put into RoboClam
E_{out} = energy expended by RoboClam
$E_{\text{potential}}$ = energy lost to change in potential energy
E_{soil} = energy lost to soil deformation
F = vertical force
$F_{i,\text{friction}}$ = measured friction force in in/out piston
$F_{u,\text{friction}}$ = measured friction force in up/down piston
H = horizontal force
h_{fluid} = height of fluidized region
h_{settle} = height of settled fluid
m_i = total mass moving during in/out stroke
m_p = mass of soil particle
m_u = total mass moving during up/down stroke
n = exponent derived from Archimedes number
N = normal force
T = input vertical force
TR = transmission ratio
t_{min} = minimum contraction time
t_{settle} = settling time
v_p = velocity of soil particle
v_s = settling velocity
v_v = velocity of valve contraction
z = depth
α = power law exponent
δ = displacement
δ_x = horizontal displacement over one stroke
δ_y = vertical displacement over one stroke
δ_1 = position at start of stroke
δ_2 = position at end of stroke
Δp_i = pressure difference over in/out piston
Δp_u = pressure difference over up/down piston
η = efficiency
θ = wedge angle
μ = coefficient of friction
μ_f = viscosity of fluid
ρ_f = density of fluid
ϕ = void fraction
ϕ_{fluid} = minimum void fraction for fluidization
ϕ_{settle} = void fraction of settled particles

References

[1] Winter, V, A. G., Deits, R., and Hosoi, A. E., 2012, "Localized Fluidization Burrowing Mechanics of Ensis Directus," J. Exp. Biol., **215**(12), pp. 2072–2080.
[2] Terzaghi, K., Peck, R., and Mesri, G., 1996, *Soil Mechanics in Engineering Practice*, 3rd, ed., Wiley, New York.
[3] Robertson, P. K., and Campanella, R. G., 1983, "Interpretation of Cone Penetration Tests. Part I: Sand," Can. Geotech. J., **20**(4), pp. 718–733.
[4] Trueman, E., 1975, *The Locomotion of Soft-Bodied Animals*, Edward Arnold, London.
[5] Rosenberg, R., and Ringdahl, K., 2005, "Quantification of Biogenic 3-D Structures in Marine Sediments," J. Exp. Mar. Biol. Ecol., **326**(1), pp. 67–76.
[6] Trueman, E., 1966, "The Dynamics of Burrowing of Some Common Littoral Bivalves," J. Exp. Biol., **44**, pp. 469–492.
[7] Dorgan, K. M., Jumars, P. A., Johnson, B., Boudreau, B. P., and Landis, E., 2005, "Burrowing Mechanics: Burrow Extension by Crack Propagation," Nature, **433**(7025), pp. 475–475.
[8] Aoyama, J., Shinoda, A., Sasai, S., Miller, M. J., and Tsukamoto, K., 2005, "First Observations of the Burrows of Anguilla Japonica," J. Fish Biol., **67**(6), pp. 1534–1543.

[9] Atkinson, R. J. A., Pelster, B., Bridges, C. R., Taylor, A. C., and Morris, S., 1987, "Behavioral and Physiological Adaptations to a Burrowing Lifestyle in the Snake Blenny, Lumpenus Lampretaeformis, and the Red Band-Fish, Cepola Rubescens," J. Fish Biol., **31**(5), pp. 639–659.
[10] Wallace, H. R., 1968, "The Dynamics of Nematode Movement," Ann. Rev. Pathol., **6**, pp. 91–114.
[11] Jung, S., 2010, "Caenorhabditis Elegans Swimming in a Saturated Particulate System," Phys. Fluids, **22**, p. 031903.
[12] Winter, V, A. G., Deits, R., and Dorsch, D., 2013, "Critical Timescales for Burrowing in Undersea Substrates Via Localized Fluidization, Demonstrated by RoboClam: A Robot Inspired by Atlantic Razor Clams," ASME Paper No. DETC2013-12798, pp. V06AT07A007.
[13] Trueman, E. R., 1966, "Bivalve Mollusks: Fluid Dynamics of Burrowing," Science, **152**(3721), pp. 523–525.
[14] Trueman, E. R., 1967, "The Dynamics of Burrowing in Ensis (bivalvia)," Proc. R. Soc. London B Biol. Sci., **166**(1005), pp. 459–476.
[15] Winter, V, A. G., Deits, R., Dorsch, D., Slocum, A., and Hosoi, A. E., 2014, "Razor Clam to RoboClam: Burrowing Drag Reduction Mechanisms and Their Robotic Adaptation," Bioinspiration Biomimetics, **9**(3), pp. 4–5.
[16] Holland, A. F., and Dean, J. M., 1977, "The Biology of the Stout Razor Clamtagelus Plebeius: I. Animal-Sediment Relationships, Feeding Mechanism, and Community Biology," Chesapeake Sci., **18**(1), pp. 58–66.
[17] Energizer Battery Company, 2009, "Energizer E91 AA Battery Product Datasheet," Energizer Holdings, Inc., St. Louis, MO.
[18] Winter, V, A. G., 2008, "Drag Reduction Mechanisms Employed by Burrowing Razor Clams (Ensis Directus)," 61st Annual Meeting of the American Physical Society Division of Fluid Dynamics, San Antonio, TX, Nov. 23, 2008.
[19] Winter, V, A. G., and Hosoi, A. E., 2011, "Identification and Evaluation of the Atlantic Razor Clam (Ensis Directus)," Integr. Comp. Biol., **51**(1), pp. 151–157.
[20] Kundu, P., and Cohen, I., 2004, *Fluid Mechanics*, 3rd, ed., Elsevier Academic Press, San Diego, CA.
[21] Lambe, T., and Whitman, R., 1969, *Soil Mechanics*, Wiley, New York.
[22] Slocum, A., 1992, *Precision Machine Design*, Society of Manufacturing Engineers, Dearborn, MI.
[23] Avallone, E. A., and Baumeister, T., III, 1996, *Marks' Standard Handbook for Mechanical Engineers*, 10th, ed., McGraw-Hill, New York.
[24] Winter, V, A. G., Hosoi, A. E., Slocum, A., and Dorsch, D., 2009, "The Design and Testing of RoboClam A Machine Used to Investigate and Optimize Razor Clam-Inspired Burrowing Mechanisms for Engineering Applications," ASME Paper No. DETC2009-86808, pp. 721–726.
[25] Richardson, J., and Zaki, W., 1954, "Sedimentation and Fluidization: Part I," Chem. Eng. Res. Des., **32**(a), pp. 35–53.
[26] Khan, A., and Richardson, J., 1989, "Fluid-Particle Interactions and Flow Characteristics of Fluidized Beds and Settling Suspensions of Spherical Particles," Chem. Eng. Commun., **78**(1), pp. 111–130.
[27] Wen, C., and Yu, Y., 1966, "Mechanics of Fluidization," Chem. Eng. Prog. Symp. Ser., **62**, pp. 100–111.